

# Estimating induced-activation of SCT barrel-modules in the ATLAS radiation environment.

C. Buttar, I. Dawson, A. Moraes  
Department of Physics, University of Sheffield, UK

V. Cindro, I. Mandic  
Josef Stefan Institute, Ljubljana, Slovenia

## Abstract

One of the consequences of operating detector systems in the harsh radiation environments of the ATLAS inner-detector will be radioactivation of the components. If the levels of radioactivity and corresponding dose rates are significant, then there will be implications for any access or maintenance operations. Given in this note are predictions for the radioactivation of SCT barrel-modules in the expected radiation environment of the inner-detector, based on both calculations and measurements. It is shown that both neutron-capture and high-energy hadron reactions must be taken into account. The predictions show that, from a radiological point of view, the SCT barrel-modules should not pose any serious problems.

18th April 2002

# Contents

<b>1</b>	<b>Introduction</b>	<b>1</b>
<b>2</b>	<b>Calculation of SCT barrel-module activation.</b>	<b>2</b>
2.1	Module description and material inventory . . . . .	2
2.2	Radionuclide production . . . . .	3
2.3	Evaluating activity . . . . .	5
2.4	Calculating dose rates . . . . .	7
2.4.1	Dose rates from $\gamma$ -emitters . . . . .	7
2.4.2	Dose rates from $\beta$ -emitters . . . . .	7
2.5	Conclusions of calculational study. . . . .	9
<b>3</b>	<b>Neutron irradiation of a SCT barrel-hybrid.</b>	<b>10</b>
3.1	The Ljubljana neutron irradiation facility. . . . .	10
3.2	The hybrid irradiations. . . . .	10
3.3	Results and conclusions . . . . .	11
<b>4</b>	<b>Dose rates for the SCT barrel system</b>	<b>12</b>
4.1	Dose rates from the module-ensemble . . . . .	12
4.2	Low mass power tapes . . . . .	13
4.3	Cooling . . . . .	13
4.4	Comments concerning PPB1 and beyond . . . . .	14
<b>5</b>	<b>Discussion</b>	<b>14</b>

# 1 Introduction

One of the consequences of operating detector systems in the harsh radiation environments of the ATLAS inner-detector will be the radioactivation of the components. If the levels of radioactivity and corresponding dose rates are significant, then there will be implications for any access or maintenance operations. In addition, maintenance operations may be required on nearby detector or machine elements, for example beam-line equipment, so the relative impact of the SCT needs to be considered. A further motivation for understanding SCT activation concerns the eventual storage or disposal of the SCT-modules at the end of the detector lifetime, when any radioactive material will have to be classified.

Radionuclides are produced in the SCT modules via the inelastic interactions of hadrons with the various target nuclei comprising the modules. The hadrons originate from: 1) particles from the p-p collisions, dominated by pions, and 2) backplash from hadron cascades in the calorimeters, mainly neutrons. The radiation environment of the inner-detector has been previously studied and is described in [1]. The best known reaction responsible for producing unstable nuclides is low-energy neutron capture ( $n,\gamma$ ), but in a high-energy radiation environments spallation is also important.

Two methods have been used for obtaining information concerning the activation of SCT barrel modules:

1. Calculations were performed in which activation and dose-rate estimates were obtained based on simulations of the ATLAS radiation environment, along with detailed mass estimates of the elements comprising SCT barrel modules. This has allowed a complete picture of module activation to be obtained for all the interactions contributing to the production of unstable radionuclides. The main difficulty with this approach is to ensure that elements with high neutron-capture cross sections are accurately included in the mass estimates as even small quantities can dominate the resulting activity and dose estimates.
2. A module-hybrid was irradiated at the Ljubljana neutron facility and the resulting activation was measured. Most of the mass of elements with high neutron-capture cross sections is contained in the hybrid, therefore these measurements should give a reasonable indication of module activation from low-energy neutron capture. Although the neutron spectrum used in the irradiations is not the same as that expected in the SCT radiation environment, this can in principle be corrected for. An advantage of irradiating detector components with low-energy neutrons is that a detailed knowledge of the elemental composition can be obtained.

The results from these two complementary investigations are described in Section 2 and Section 3 respectively. An extension of the module-activation results to assess their contribution to dose-rates for the entire SCT barrel system is discussed in Section 4. It should be noted that the focus of current work has been to obtain information concerning the activation of barrel-modules and their immediate services, and not the activation of the carbon fibre support-structures, patch-panels or any other auxiliary material. However, using the results and conclusions given in this report, the radiological impact of any material not included in the current study should be relatively easy to assess once their details become known. A general discussion of the results is given in Section 5.

## 2 Calculation of SCT barrel-module activation.

### 2.1 Module description and material inventory

In order to make activation estimates, it is necessary to obtain a detailed inventory of the materials involved in the construction of a module. The relevant information is now becoming available as SCT modules go into the production phase [2]. Of particular importance is knowledge of elements containing isotopes with high neutron capture cross sections. For example,  $^{197}\text{Au}$  has a thermal neutron capture cross section  $\sim 100 \text{ b (n,}\gamma\text{)}$  and even small quantities of such an isotope can contribute considerably, or even dominate the activated environment.

In the SCT barrel-module system there are 4 concentric cylinders, comprising 32, 40, 48 and 56 rows of 12 modules respectively. Each SCT barrel module comprises silicon sensors, baseboard with BeO facings, ASICs and a Cu/polymide hybrid [3], connected to opto-packages and dog-legs [4]. Each row of modules has associated with it a cooling pipe [5] and power tape. Unfortunately, material details are not always given in their elemental form and assumptions are therefore unavoidable. For example: 1) Thermal adhesives assumed to be 70% polyimide and 30% BN; 2) Epoxy films, polyimide layers with adhesives and PEEK are chemically described as  $\text{C}_{22}\text{H}_{10}\text{N}_2\text{O}_5$ ; 3) The solder composition is assumed to be 59% Pb, 40% Sn and 1%Ag; 4) Capacitors made of AlO and resistors 20% C and 80% AlO. Perhaps the most important assumption concerns the use of silver loaded conductive glues. Silver is important due to its high thermal neutron capture cross section and the long half-life of  $^{110\text{m}}\text{Ag}$ . In the current calculations, 100 mg of silver per module is assumed based on the material estimates of [3].

In total, the module mass is calculated to weigh  $\sim 35 \text{ g}$  and contain 15 different elements. Details of the module material inventory assumed in the current calculations are given in Table 1. It should be stressed that the activation calculations given in Section 2 of this report are based entirely on the assumed material composition of Table 1.

Elements	Silicon sensors	Baseboard with BeO facings	ASIC's	Hybrid	Cooling pipe with coolant	Power tape	Opto Package / Dog Leg	Total (g)
<i>H</i>	0.001	0.011	0.002	0.042	-	0.012	0.035	0.103
<i>Be</i>	-	0.597	-	-	-	-	-	0.597
<i>B</i>	0.009	-	-	0.041	-	-	-	0.050
<i>C</i>	0.036	4.758	0.043	3.234	0.821	0.306	0.926	10.124
<i>N</i>	0.016	0.031	0.004	0.146	-	0.032	0.324	0.553
<i>O</i>	0.011	1.145	0.020	0.506	-	0.093	0.304	2.079
<i>F</i>	-	-	-	-	3.462	-	-	3.462
<i>Al</i>	-	0.118	0.028	0.393	1.166	0.780	0.434	2.919
<i>Si</i>	10.812	-	0.742	0.187	-	-	0.029	11.770
<i>Ni</i>	-	-	-	0.025	-	-	0.015	0.040
<i>Cu</i>	-	-	-	1.501	-	-	1.071	2.572
<i>Ag</i>	0.006	-	0.144	0.028	-	-	0.0004	0.178
<i>Sn</i>	-	-	-	0.049	-	-	0.012	0.061
<i>Au</i>	-	-	-	0.010	-	-	-	0.010
<i>Pb</i>	-	-	-	0.073	-	-	0.024	0.097
<i>Total (g)</i>	10.891	6.660	0.983	6.235	5.449	1.223	3.174	34.615

Table 1: Table of barrel module element masses.

## 2.2 Radionuclide production

Radionuclides are produced in the SCT modules via the inelastic interactions of hadrons with the various target nuclei comprising the modules. However, radionuclides with short half-lives can be neglected as access to the irradiated SCT material is unlikely for at least several days. In the current study, radionuclides are only considered of radiological interest if they have half-lives greater than 1 hour and less than 30 years.

Radionuclide production can be divided into two categories:

1. Production via low energy ( $< 20\text{MeV}$ ) neutron interactions, eg  $(n,\gamma)$ ,  $(n,p)$ ,  $(n,\alpha)$ ,  $(n,np)$  etc.. The cross sections for these neutron interactions are well known for all the target nuclei being considered [6]. The production probability for each radionuclide of interest, per target nuclei, can be obtained by convolving the energy dependent cross sections with neutron energy spectra. According to the studies of [1], thermal neutrons account for more than a half of the total neutron fluences in and around the SCT barrel system. In the current study, the radionuclide production probabilities were evaluated for all the low-energy neutron interactions and, as expected, the dominant process was found to be neutron capture  $(n,\gamma)$ .

Values of radionuclide production per p-p event per module from  $(n,\gamma)$  interactions are obtained simply from  $n \sum \phi_i \sigma_i$  where the sum is over all the energy bins  $i$  used in the fluence  $\phi$  predictions [1].  $n$  is the number of atoms of a given isotope in the module and  $\sigma_i$  are the corresponding  $(n,\gamma)$  cross sections [6, 7] averaged over each energy-bin. As expected, the dominant capture process is from thermal neutrons. It should be noted that the inner detector thermal neutron rate predictions ( $\sim 2 \times 10^6 \text{ n}_{th} \text{ cm}^{-2} \text{ s}^{-1}$  [1]) can be considered conservative. This is because elements such as boron, xenon, silver, gold etc., which have high thermal neutron capture cross sections, were not included. \*

2. High energy inelastic interactions, or spallation. Unlike neutron interactions, radionuclide production cross sections from spallation are not available for all the target nuclei, and are often scarce for particles such as pions. In this study, the hadron interaction models in the Monte Carlo particle transport code FLUKA [8] are used. The results then depend on the quality and coverage of the physics models, in particular: nuclear evaporation, the intranuclear cascade, nuclear fission and nuclear fragmentation. Of these the first three are considered to be well modelled but fragmentation, which is important for the heavier target nuclei, is not included in the code. The general features of residual-nuclei production predicted by FLUKA are in reasonable agreement with experimental data [9], except for light-nuclei production from heavy targets where fragmentation effects start becoming important. Fortunately, the bulk of the target nuclei in SCT modules are in the light to medium mass range. However, for single isotope prediction, a factor  $\sim 2$  is probably a reasonable measure of the uncertainties in the predictions.

Given in Table 2 are the details of the isotopes considered in the calculations to understand radionuclide production due to  $(n,\gamma)$  interactions. Included are the decay data used for calculating dose-rates. Similar data for the production of radionuclides via spallation, as predicted by FLUKA, are presented in Table 3.

---

\*This also means that the contribution to inner-detector photon fluences from  $(n,\gamma)$  interactions will be underestimated, the implications of which needs to be checked. However, this has no consequence for activation issues.

Isotope (% of natural abundance)	Mass per module (g)	Produced nuclide $\sigma(n_{th}, \gamma)$ (b)	Half-life	Principal decay mode(s) and energies	Production per p-p event per module
$^2\text{H}$ (0.015%)	$1.55 \times 10^{-5}$	$^3\text{H}$ (0.00055)	12.35 y	100% $\beta^-$ , $E_{ave} = 5.68$ keV	$6.28 \times 10^{-12}$
$^{30}\text{Si}$ (3.10%)	0.365	$^{31}\text{Si}$ (0.107)	2.62 h	99.9% $\beta^-$ , $E_{ave} = 0.596$ MeV	$5.41 \times 10^{-6}$
$^{63}\text{Cu}$ (69.17%)	1.779	$^{64}\text{Cu}$ (4.50)	12.7 h	44.9% Electron capture 17.9% $\beta^+$ , $E_{ave} = 0.278$ MeV 37.2% $\beta^-$ , $E_{ave} = 0.190$ MeV 0.49% $\gamma$ , $E = 1.346$ MeV	$2.04 \times 10^{-4}$
$^{64}\text{Ni}$ (0.926%)	$3.70 \times 10^{-4}$	$^{65}\text{Ni}$ (1.52)	2.52 h	28.1% $\beta^-$ , $E_{ave} = 0.221$ MeV 9.8% $\beta^-$ , $E_{ave} = 0.372$ MeV 60.7% $\beta^-$ , $E_{ave} = 0.875$ MeV 4.61% $\gamma$ , $E = 0.366$ MeV 14.8% $\gamma$ , $E = 1.116$ MeV 23.5% $\gamma$ , $E = 1.482$ MeV	$1.29 \times 10^{-8}$
$^{109}\text{Ag}$ (48.16%)	0.086	$^{110m}\text{Ag}$ (4.7)	249.9 d	67.5% $\beta^-$ , $E_{ave} = 0.0218$ MeV 30.6% $\beta^-$ , $E_{ave} = 0.166$ MeV 94.7% $\gamma$ , $E = 0.658$ MeV 10.7% $\gamma$ , $E = 0.678$ MeV 16.7% $\gamma$ , $E = 0.707$ MeV 22.4% $\gamma$ , $E = 0.764$ MeV 72.9% $\gamma$ , $E = 0.885$ MeV 34.3% $\gamma$ , $E = 0.938$ MeV 24.3% $\gamma$ , $E = 1.384$ MeV 13.1% $\gamma$ , $E = 1.505$ MeV	$7.24 \times 10^{-6}$
$^{112}\text{Sn}$ (0.97%)	$5.92 \times 10^{-4}$	$^{113}\text{Sn}$ (0.4)	115.1 d	100% Electron capture 1.85% $\gamma$ , $E = 0.255$ MeV 38.9% X-ray, $E = 0.024$ MeV 20.7% X-ray, $E = 0.024$ MeV	$2.51 \times 10^{-8}$
$^{120}\text{Sn}$ (32.6%)	0.020	$^{121}\text{Sn}$ (0.16)	1.13 d	100% $\beta^-$ , $E_{ave} = 0.383$ MeV	$1.79 \times 10^{-7}$
$^{124}\text{Sn}$ (5.79%)	$3.53 \times 10^{-3}$	$^{125}\text{Sn}$ (0.004)	9.64 d	2.82% $\beta^-$ , $E_{ave} = 0.468$ MeV 83.0% $\beta^-$ , $E_{ave} = 0.940$ MeV 3.92% $\gamma$ , $E = 0.822$ MeV 3.92% $\gamma$ , $E = 0.916$ MeV 8.90% $\gamma$ , $E = 1.067$ MeV 4.18% $\gamma$ , $E = 1.089$ MeV 2.14% $\gamma$ , $E = 2.002$ MeV	$2.28 \times 10^{-9}$
$^{197}\text{Au}$ (100%)	0.010	$^{198}\text{Au}$ (98.7)	2.70 d	98.7% $\beta^-$ , $E_{ave} = 0.315$ MeV 95.5% $\gamma$ , $E = 0.412$ MeV	$1.55 \times 10^{-5}$
$^{208}\text{Pb}$ (52.4%)	0.051	$^{209}\text{Pb}$ (0.0005)	3.25 h	100% $\beta^-$ , $E_{ave} = 0.198$ MeV	$1.74 \times 10^{-9}$
Additional Isotopes Considered					
$^{58}\text{Fe}$ (0.28%)	$2.8 \times 10^{-6}$	$^{59}\text{Fe}$ (1.15)	44.5 d	52.8% $\beta^-$ , $E_{ave} = 0.149$ MeV 45.6% $\beta^-$ , $E_{ave} = 0.081$ MeV 56.1% $\gamma$ , $E = 1.099$ MeV 43.6% $\gamma$ , $E = 1.292$ MeV	$8.92 \times 10^{-10}$
$^{59}\text{Co}$ (100%)	0.001	$^{60}\text{Co}$ (16.5)	5.27 y	99.9% $\beta^-$ , $E_{ave} = 0.0958$ MeV 99.9% $\gamma$ , $E = 1.173$ MeV 100% $\gamma$ , $E = 1.332$ MeV	$4.37 \times 10^{-7}$
$^{81}\text{Br}$ (49.31%)	$4.93 \times 10^{-4}$	$^{82}\text{Br}$ (0.27)	1.47 d	98.6% $\beta^-$ , $E_{ave} = 1.378$ MeV 70.8% $\gamma$ , $E = 0.554$ MeV 43.5% $\gamma$ , $E = 0.619$ MeV 28.5% $\gamma$ , $E = 0.698$ MeV 83.6% $\gamma$ , $E = 0.777$ MeV 24.0% $\gamma$ , $E = 0.828$ MeV 27.2% $\gamma$ , $E = 1.044$ MeV 26.5% $\gamma$ , $E = 1.317$ MeV 16.3% $\gamma$ , $E = 1.475$ MeV	$1.00 \times 10^{-8}$

Table 2: Details of the isotopes considered in the calculations to understand radionuclide production due to (n, $\gamma$ ) reactions. Included are the decay data used for calculating dose-rates.

In addition to the elements listed in Table 1, the analysis of neutron activation has also been extended to include Fe, Co and Br, as shown in Table 2. These elements have appreciable neutron-capture cross sections and are often present in materials used in the electronics industry. Therefore, 1 mg of each of these elements were included in the study in order to investigate the effects of such elements to activity levels and also, to facilitate any future scaling to actual masses, should any of these materials come to be used in the module construction.

Nuclide	Half-life	Principal decay mode(s) and energies	Production per p-p event per barrel-module
$^3\text{H}$	12.35 y	100% $\beta^-$ , $E_{\alpha\vee e} = 5.68$ keV	$4.85 \times 10^{-5}$
$^7\text{Be}$	53.3 d	100% Electron capture 10.3% $\gamma$ , $E = 0.478$ MeV	$1.26 \times 10^{-5}$
$^{22}\text{Na}$	2.60 y	10.2% Electron capture 89.8% $\beta^+$ $E_{\alpha\vee e} = 0.215$ MeV 100% $\gamma$ , $E = 1.275$ MeV	$1.07 \times 10^{-5}$
$^{24}\text{Na}$	15.0 h	99.9% $\beta^-$ $E_{\alpha\vee e} = 0.554$ MeV 100% $\gamma$ , $E = 1.369$ MeV 99.9% $\gamma$ , $E = 2.754$ MeV	$2.34 \times 10^{-6}$
$^{32}\text{P}$	14.3 d	100% $\beta^-$ $E_{\alpha\vee e} = 0.695$ MeV	$3.52 \times 10^{-8}$
$^{48}\text{V}$	16.2 d	50% Electron capture 50% $\beta^+$ $E_{\alpha\vee e} = 0.291$ MeV 100% $\gamma$ $E = 0.984$ MeV 97.5% $\gamma$ $E = 1.312$ MeV	$1.76 \times 10^{-7}$
$^{54}\text{Mn}$	312.5 d	100% Electron capture 100% $\gamma$ , $E = 0.835$ MeV	$1.06 \times 10^{-6}$
$^{59}\text{Fe}$	44.5 d	52.8% $\beta^-$ $E_{\alpha\vee e} = 0.149$ MeV 45.6% $\beta^-$ $E_{\alpha\vee e} = 0.081$ MeV 56.1% $\gamma$ , $E = 1.099$ MeV 43.6% $\gamma$ , $E = 1.292$ MeV	$1.41 \times 10^{-7}$
$^{56}\text{Co}$	78.8 d	80.1% Electron capture 18.8% $\beta^+$ $E_{\alpha\vee e} = 0.632$ MeV 100% $\gamma$ , $E = 0.847$ MeV 14.1% $\gamma$ , $E = 1.038$ MeV 67.0% $\gamma$ , $E = 1.238$ MeV 15.5% $\gamma$ , $E = 1.771$ MeV 7.77% $\gamma$ , $E = 2.035$ MeV 16.7% $\gamma$ , $E = 2.599$ MeV	$3.87 \times 10^{-7}$
$^{57}\text{Co}$	270.9 d	100% Electron capture 85.6% $\gamma$ , $E = 0.122$ MeV 10.6% $\gamma$ , $E = 0.137$ MeV	$1.41 \times 10^{-6}$
$^{58}\text{Co}$	70.8 d	85.0% Electron capture 15.0% $\beta^+$ $E_{\alpha\vee e} = 0.201$ MeV 99.4% $\gamma$ , $E = 0.811$ MeV	$1.39 \times 10^{-6}$
$^{60}\text{Co}$	5.27 y	99.9% $\beta^-$ $E_{\alpha\vee e} = 0.0958$ MeV 99.9% $\gamma$ , $E = 1.173$ MeV 100% $\gamma$ , $E = 1.332$ MeV	$4.40 \times 10^{-7}$
$^{64}\text{Cu}$	12.7 h	44.9% Electron capture 17.9% $\beta^+$ $E_{\alpha\vee e} = 0.278$ MeV 37.2% $\beta^-$ $E_{\alpha\vee e} = 0.190$ MeV 0.49% $\gamma$ , $E = 1.346$ MeV	$1.44 \times 10^{-6}$

Table 3: Details of unstable radionuclide production in the SCT barrel modules due to spallation interactions, as predicted by FLUKA. Included are the decay data used for calculating dose-rates.

## 2.3 Evaluating activity

Knowledge of the various radionuclide production rates along with their half-lives allows the calculation of radioactivities; defined as the number of decays per second. The build-up and decay of activity, for each radionuclide, is given by:

$$A = N \phi (1 - e^{-\lambda t_i}) e^{-\lambda t_c} \quad (1)$$

where  $t_i$  and  $t_c$  are irradiation and cooling times respectively.  $N$  is the number of produced radionuclides per p-p event per module,  $\phi$  is the average number of p-p events per second and  $\lambda$  is the decay constant. In going from radionuclide production per p-p event to activity, it is necessary to make certain assumptions about the p-p event rates. The design luminosity of the *LHC* is  $10^{34} \text{ cm}^{-2} \text{ s}^{-1}$ , resulting in a p-p interaction rate of  $8 \times 10^8 \text{ s}^{-1}$  as predicted by PHOJET [10]. However, the average luminosity over longer timescales will be less due to beam-lifetimes etc. and an averaged luminosity value of  $5 \times 10^{33} \text{ cm}^{-2} \text{ s}^{-1}$  is assumed [11].

Shown in Figure 1 are the dominant contributions to activation from (n, $\gamma$ ) and spallation reactions. Presented in Table 4 are activities obtained 1 day, 1 week and 1 month after shutdown, for the two cases of one-year of high-luminosity running and ten-years of high luminosity running. A high-luminosity year is defined as 180 days of running (assuming the average beam-luminosity of  $5 \times 10^{33} \text{ cm}^{-2} \text{ s}^{-1}$ ) followed by 185 days of shutdown.

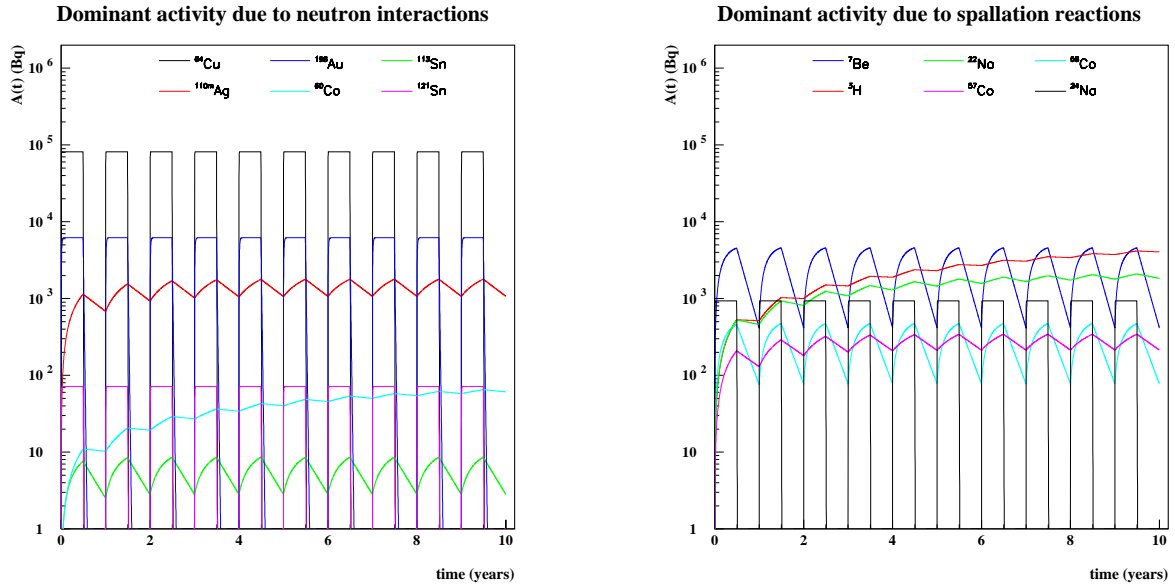


Figure 1: Dominant activities.

Radionuclide	Dominant activities (Bq) per SCT-barrel module					
	180 days irradiating cooling times			10 years irradiating cooling times		
	1day	1week	1month	1day	1week	1month
<sup>3</sup> H	529.51	529.02	527.16	4166.95	4163.10	4148.41
<sup>7</sup> Be	4496.06	4158.58	3083.51	4535.43	4194.99	3110.51
<sup>22</sup> Na	526.89	524.59	515.85	2094.96	2085.80	2051.05
<sup>24</sup> Na	341.22	0.43	-	341.22	0.43	-
<sup>31</sup> Si	3.78	-	-	3.78	-	-
<sup>32</sup> P	13.41	10.03	3.29	13.41	10.03	3.29
<sup>48</sup> V	67.42	52.16	19.49	67.42	52.16	19.49
<sup>54</sup> Mn	139.26	137.42	130.59	250.86	247.55	235.24
<sup>56</sup> Co	121.94	115.67	94.49	127.07	120.54	98.46
<sup>57</sup> Co	207.62	204.46	192.78	342.03	336.82	317.57
<sup>58</sup> Co	456.07	430.05	343.34	469.24	442.47	353.26
<sup>59</sup> Fe	52.49	47.81	33.41	52.67	47.97	33.53
<sup>60</sup> Co	22.02	21.98	21.79	130.73	130.59	129.38
<sup>64</sup> Cu	22114.09	8.54	-	22114.09	8.54	-
<sup>65</sup> Ni	0.01	-	-	0.01	-	-
<sup>82</sup> Br	2.49	0.15	-	2.49	0.15	-
<sup>110m</sup> Ag	1135.04	1116.31	1047.32	1782.76	1753.33	1644.97
<sup>113</sup> Sn	6.60	6.37	5.55	7.43	7.17	6.24
<sup>121</sup> Sn	38.77	0.98	-	38.77	0.98	-
<sup>125</sup> Sn	0.85	0.55	0.11	0.85	0.55	0.11
<sup>198</sup> Au	4796.22	1027.88	2.80	4796.22	1027.88	2.80

Table 4: Activation per SCT barrel module for different irradiation and cool-down times.



## 2.4 Calculating dose rates

Dose rates are obtained at distances of 10 cm, 30 cm and 100 cm from the centre of a barrel-module. The calculations are facilitated by assuming each module is a point source of radioactivity. This assumption is good for the distances larger than the dimensions of the module (ie 30 cm and 100 cm) and will be conservative by some  $\sim 30\%$  for the value obtained at 10 cm.

### 2.4.1 Dose rates from $\gamma$ -emitters

The dose rate  $D_\gamma$  from a  $\gamma$ -emitting nuclide can be obtained [12], for a point source, from:

$$D_\gamma = \frac{A \cdot E}{7d^2} \quad \mu Sv/h \quad (2)$$

where  $A$  is the activity in MBq,  $E$  is the sum of  $\gamma$  energies in MeV weighted by their emission probabilities and  $d$  is the distance from the source in metres. The above formula is valid for photons in the range 0.05 to 2 MeV, which is the range covering most of the emitted  $\gamma$ s. Using the activity values given in Table 4 and the relevant gamma decay and energy information from Tables 2 and 3, the total gamma dose rate is obtained by summing the contributions from each radionuclide using equation 2. The results are given in Table 5.

### 2.4.2 Dose rates from $\beta$ -emitters

The dose rate  $D_\beta$  from a  $\beta$ -emitting nuclide can be approximated [12] by:

$$D_\beta = \frac{10 A}{d^2} \quad \mu Sv/h \quad (3)$$

This expression assumes no absorption of the  $\beta$ s, which can be appreciable depending on the  $\beta$  energy. For example, the average  $\beta$  energy in  $^3\text{H}$  decay is 5.68 keV. The range in air of such  $\beta$ s is a few mm and will not contribute to external  $\beta$ -doses. However, most of the emitted  $\beta$ s have much higher energies, with ranges in air going up to several metres. In order to avoid overly overestimating the  $\beta$ -doses, the maximum ranges in air of all  $\beta$ -emitters have been obtained and, if the range is shorter than the distance at which the dose is calculated, then it is not included in the total  $\beta$ -dose estimate. In addition to the ranges in air, the self-shielding of  $\beta$ s in the module-material should also be taken into account. An obvious example of this is  $\beta$  attenuation from  $^{110m}\text{Ag}$  decays. Most of the silver in the module design is found in the conductive glues between the ASICs and the hybrid. There is at least  $\sim 0.5$  mm of ASIC-silicon to traverse which, according to [14], will completely attenuate the  $\beta$ s with maximum energy 87 keV, and only  $\sim 3\%$  of the  $\beta$ s with maximum energy 531 keV will escape. In the current  $\beta$ -dose calculations it is assumed that 90% of the total module silver is shielded and that the associated  $\beta$ s are completely absorbed. The results are given in Table 6. This strategy will still, however, overestimate  $\beta$ -doses for two reasons; 1) the ranges in air are obtained assuming the maximum  $\beta$ -energy and 2) self-shielding of the module material has only been considered for  $^{110m}\text{Ag}$ . The  $\beta$ -dose estimates should therefore be considered as upper-limits.

Radionuclide	$\gamma$ dose (nSv/h) at 1 m for a single SCT-barrel module					
	180 days irradiating cooling times			10 years irradiating cooling times		
	1day	1week	1month	1day	1week	1month
<sup>7</sup> Be	0.032	0.029	0.022	0.032	0.030	0.022
<sup>22</sup> Na	0.165	0.164	0.162	0.656	0.653	0.643
<sup>24</sup> Na	0.201	-	-	0.201	-	-
<sup>48</sup> V	0.027	0.021	0.008	0.027	0.021	0.008
<sup>54</sup> Mn	0.017	0.016	0.016	0.030	0.029	0.028
<sup>56</sup> Co	0.050	0.048	0.039	0.052	0.050	0.041
<sup>57</sup> Co	0.004	0.003	0.003	0.006	0.006	0.005
<sup>58</sup> Co	0.062	0.059	0.047	0.064	0.061	0.048
<sup>59</sup> Fe	0.009	0.008	0.006	0.009	0.008	0.006
<sup>60</sup> Co	0.008	0.008	0.008	0.047	0.047	0.046
<sup>64</sup> Cu	0.581	-	-	0.581	-	-
<sup>82</sup> Br	0.001	-	-	0.001	-	-
<sup>110m</sup> Ag	0.403	0.396	0.372	0.633	0.622	0.584
<sup>198</sup> Au	0.269	0.058	-	0.269	0.058	-
<i>Total</i>	1.830	0.811	0.683	2.609	1.586	1.431

Table 5: Dominant isotopic contributions to  $\gamma$  doses.

Radionuclide	$\beta$ dose (nSv/h) at 1 m for a single SCT-barrel module					
	180 days irradiating cooling times			10 years irradiating cooling times		
	1day	1week	1month	1day	1week	1month
<sup>24</sup> Na	3.41	-	-	3.41	-	-
<sup>31</sup> Si	0.04	-	-	0.04	-	-
<sup>32</sup> P	0.13	0.10	0.03	0.13	0.10	0.03
<sup>59</sup> Fe	0.29	0.26	0.18	0.29	0.26	0.18
<sup>60</sup> Co	-	-	-	-	-	-
<sup>64</sup> Cu	221.14	0.09	-	221.14	0.09	-
<sup>82</sup> Br	0.02	-	-	0.02	-	-
<sup>110m</sup> Ag	0.35	0.34	0.32	0.55	0.54	0.50
<sup>121</sup> Sn	0.39	0.01	-	0.39	0.01	-
<sup>125</sup> Sn	0.01	0.01	-	0.01	0.01	-
<sup>198</sup> Au	47.96	10.28	0.03	47.96	10.28	0.03
<i>Total</i>	274	11.1	0.56	274	11.3	0.74

Table 6: Dominant isotopic contributions to  $\beta$  doses.

Distance from the source	$\gamma$ ( $\beta$ ) dose rates in nSv/h for one SCT-barrel module					
	180 days irradiating cooling times			10 years irradiating cooling times		
	1day	1week	1month	1day	1week	1month
10 cm	183 (27420)	81 (1150)	68 (90)	261 (27550)	159 (1280)	143 (220)
30 cm	20 (3040)	9.0 (120)	8.0 (6.0)	29 (3040)	18 (130)	16 (8.0)
1 m	1.83 (274)	0.81 (11)	0.68 (0.6)	2.61 (274)	1.59 (11)	1.43 (0.7)

Table 7: Module  $\gamma$  and  $\beta$  dose rates at different distances.

## 2.5 Conclusions of calculational study.

Concerning (n, $\gamma$ ) activation the dominant radionuclides are  $^{64}\text{Cu}$ ,  $^{198}\text{Au}$  and  $^{110m}\text{Ag}$ , as illustrated in Figure 1. However,  $^{64}\text{Cu}$  and  $^{198}\text{Au}$  have half-lives of 12.7 hours and 2.7 days respectively. On timescales greater than a week, when the  $^{198}\text{Au}$  activity becomes small,  $^{110m}\text{Ag}$  will dominate ( $t_{1/2} = 249.9$  days).

Concerning spallation induced activation, the dominant radionuclides are  $^3\text{H}$ ,  $^7\text{Be}$ ,  $^{22}\text{Na}$  and  $^{24}\text{Na}$ . However, when considering external dose rates from activation,  $^3\text{H}$  can be neglected as discussed in Section 2.4.2. Also, the principle decay mode of  $^7\text{Be}$  is electron-capture with no associated gammas.  $^{24}\text{Na}$  has a relatively short half-life thus leaving  $^{22}\text{Na}$  ( $t_{1/2} = 2.6$  years) as the most important radionuclide produced in high-energy inelastic interactions. Interestingly, the target nuclei mainly responsible for  $^{22}\text{Na}$  production is silicon and is therefore unavoidable.

The dominant radionuclides that will contribute to  $\gamma$ -doses several days after shutdown are  $^{22}\text{Na}$  and  $^{110m}\text{Ag}$ . As for  $\beta$ -doses,  $^{64}\text{Cu}$  is significant in the first few days but quickly decays, leaving  $^{198}\text{Au}$  to dominate module activity. However, on timescales longer than a week when the  $^{198}\text{Au}$  disappears,  $\beta$ -doses become comparable to the  $\gamma$ -doses. As the  $\beta$ -doses are considered overestimates, it is reasonable to conclude that  $\gamma$ -doses eventually dominate the module dose-rates.

Inspection of Table 7 shows that after 10 years of LHC running the module  $\gamma$ -doses will be  $\sim 0.2\mu\text{Sv/h}$  at a distance of 10 cm. The corresponding  $\beta$ -doses are much higher for the first week after shutdown but become comparable to the  $\gamma$ -doses after a couple of weeks. According to the CERN radiation safety manual [15], radioactive materials with dose rates less than  $0.1\mu\text{Sv/h}$  at 10 cm are considered *non-radioactive*, while dose rates above  $0.1\mu\text{Sv/h}$  but less than  $10\mu\text{Sv/h}$  at 10 cm are considered *slightly-radioactive*. After several years of LHC running and several days shutdown, individual SCT barrel modules will probably fall into the category of being *slightly-radioactive*.

### 3 Neutron irradiation of a SCT barrel-hybrid.

It can be seen from the module material inventory in Table 1 that a good fraction of the module mass is found in the hybrid + ASICs ( $\sim 20\%$ ), covering a wide range of elements. More importantly, the hybrid contains nearly all the mass of elements that have high neutron capture cross sections such as gold and silver. Therefore, irradiating the SCT barrel-hybrids with low-energy neutrons should give a reliable indication of overall module activation from  $(n,\gamma)$  processes. This has been done at the Ljubljana reactor facility [16].

#### 3.1 The Ljubljana neutron irradiation facility.

The Ljubljana neutron irradiation facility is an experimental nuclear reactor of the type TRIGA. Samples are irradiated by placing them into the core through a tube which occupies a fuel rod position. The ATLAS group uses two such irradiation tubes which are located towards the outside of the core. The tubes have different dimensions: the small tube has a circular cross section with 2.2 cm diameter and the large tube has an elliptic cross section with axis lengths 7 cm and 5 cm. The irradiation tubes enter the core from above and are about 5m long because the core is covered with 5m of water. The tubes are curved in a chicane just above the core to prevent radiation from the core escaping through the tube. The chicane limits the length of the sample to be irradiated to about 15cm.

The reactor can be run with a large range of operating powers (a few W to 250 kW), enabling irradiations with various neutron fluxes. For example, previous irradiations of ATLAS electronics was done in the big tube at a reactor power of 25 kW, corresponding to a fluence of  $1 \times 10^{13} \text{ n/cm}^2$  being reached in 22 seconds. The neutron energy spectrum in the tube has been determined by measuring the activation of foils of different materials and comparing with simulations [16, 17].

#### 3.2 The hybrid irradiations.

An SCT barrel-hybrid with 12 (new epi) ABCD3T chips was irradiated with a total neutron fluence of  $2 \times 10^{14} \text{ n cm}^{-2}$  (1 MeV-equivalent), corresponding approximately to the expected fluence over the lifetime of the experiment. The energy spectrum in these irradiations was such that the thermal neutron fluence was  $\sim 1.5$  greater than the fast ( $E > 100 \text{ keV}$ ) neutron fluence, resulting in a total thermal neutron fluence of  $3 \times 10^{14} \text{ n cm}^{-2}$  [17]. The irradiation time was  $\sim 440 \text{ s}$ .

Gamma spectroscopy was done on the irradiated hybrid 21 days after the irradiations, allowing the activities of the dominant isotopes to be measured. In addition, knowledge of isotopic activity and the total thermal neutron fluence allows the corresponding elemental masses to be derived. The results of the spectroscopy are given in Table 8.

Identified isotope	Half-life (days)	Measured activity (Bq)	$\sigma_{th}$ (barns) of parent	Isotopic mass (mg)	Elemental mass (mg)
$^{110m}\text{Ag}$	249.9	8400	4.7	35.6	74
$^{198}\text{Au}$	2.7	17000	98.7	13.8	13.8
$^{58}\text{Co}$	70.9	370	-	-	-
$^{60}\text{Co}$	1923.0	880	16.0	4.4	4.4
$^{124}\text{Sb}$	60.2	72	4.0	0.12	0.28
$^{113}\text{Sn}$	115.1	88	0.4	2.2	230
$^{65}\text{Zn}$	244.1	200	0.76	3.0	6.2

Table 8: Measured hybrid activities and elemental mass estimates. The activities are accurate to 20%

### 3.3 Results and conclusions

The measured activities obtained from gamma spectroscopy are listed in Table 8. The mass of the activated hybrid elements can be estimated using the thermal neutron capture cross sections along with the corresponding isotopic fractions. It should be noted, however, that the mass estimates are obtained assuming the isotopes are produced via thermal-neutron capture. In some cases other reaction channels may be involved resulting in an overestimate of the mass. For example, some  $\sim 30\%$  of  $^{198}\text{Au}$  production in the Ljubljana reactor is expected to occur via resonance capture.  $^{110m}\text{Ag}$  production on the other hand is dominated by thermal-neutron capture in the Ljubljana irradiations.

The dominant isotopes produced in the hybrid neutron irradiations are  $^{110m}\text{Ag}$ , and  $^{198}\text{Au}$ . The estimated masses of the corresponding elements are 74 mg and 13.8 mg respectively. Also of radiological interest is the small quantity of cobalt in the hybrid, giving rise to  $^{60}\text{Co}$ . Its long half-life will mean that the SCT modules will be classified as radioactive many years after the shutdown of the LHC. See Section 5 for further discussion. The spectroscopy also revealed the presence of Bromine, which is known to exist in the hybrid-holder in significant amounts. However, its presence in small quantities in the hybrid cannot be ruled out.

Also measured was the  $\gamma$  dose-rate of the hybrid at a distance of  $\sim 10\text{cm}$ , using a Berthold (LB1236) counter, 45 and 81 days after the initial irradiation. It was found to be  $\sim 0.8 \mu\text{Sv/h}$  and  $\sim 0.35 \mu\text{Sv/h}$  respectively.

## 4 Dose rates for the SCT barrel system

### 4.1 Dose rates from the module-ensemble

It is of interest to estimate the total dose rate from all the barrel-modules comprising the SCT barrel system. This has been done by extending the results of the calculations, as described in Section 2, by assuming every module in the barrel system is a point source of identical activation. This method should overestimate the corresponding dose-rate predictions because 1) the spallation induced activation estimates for the barrel modules were obtained assuming the high-energy particle rates at the inner-barrel layer and 2) apart from silver, self-shielding of  $\beta$ s has not been taken into account. Two ‘access scenarios’ are considered, shown in Figure 2. The corresponding results are given in Table 9 and Table 10.

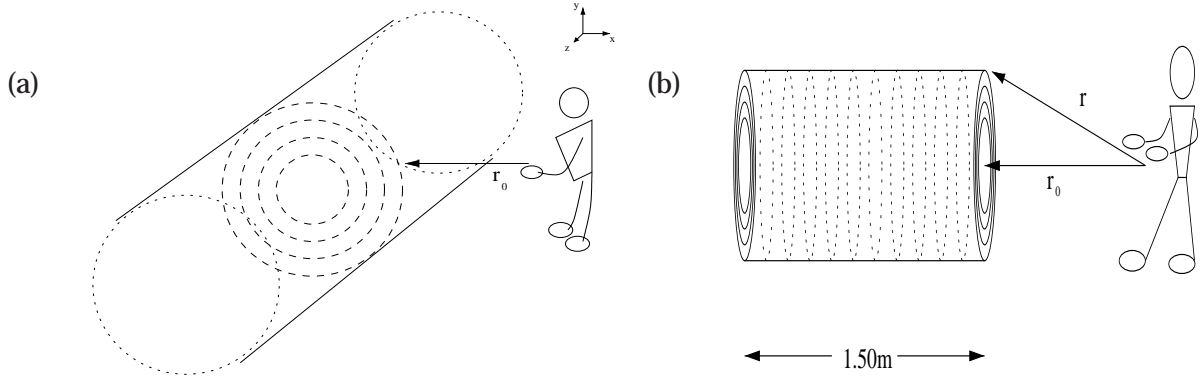


Figure 2: Considered access scenarios (a) Scenario 1 and (b) Scenario 2.

Distance of closest approach	Maximum $\gamma$ ( $\beta$ ) doses in $\mu\text{Sv/h}$ for Scenario 1								
	180 days irradiating cooling times						10 years irradiating cooling times		
	1day	1week	1month	1day	1week	1month	1day	1week	1month
10 cm	10 (1558)	4.6 (63)	3.9 (3.2)	15 (1559)	9.0 (64)	8.1 (4.2)			
30 cm	5.8 (866)	2.6 (35)	2.2 (1.7)	8.3 (867)	5.0 (35)	4.5 (2.3)			
100 cm	1.7 (248)	0.8 (9.8)	0.6 (0.2)	2.4 (248)	1.5 (9.9)	1.3 (0.3)			

Table 9: Scenario 1

Inspection of Tables 9 and 10 show that after several days cool-down time,  $\gamma$ -doses will be less than  $\sim 10 \mu\text{Sv/h}$  at 10 cm. The corresponding  $\beta$ -dose values are high after one day ( $\sim 1.0 \text{ mSv/h}$ ) but quickly fall to less than  $100 \mu\text{Sv/h}$  after 1 week. However, as already discussed, self-shielding of the modules has not been fully taken into account and  $\beta$ -dose rates should be considered as conservative upper limits. After 1 month cool-down the total barrel system dose rate at 10 cm will be less than  $10 \mu\text{Sv/h}$ . If the dose rate is greater than  $10 \mu\text{Sv/h}$  but less than

Distance of closest approach	Maximum $\gamma$ ( $\beta$ ) doses in $\mu\text{Sv/h}$ for Scenario 2								
	180 days irradiating cooling times						10 years irradiating cooling times		
	1day	1week	1month	1day	1week	1month	1day	1week	1month
10 cm	7.1 (1056)	3.1 (42)	2.6 (2.1)	10.1 (1056)	6.1 (43)	5.5 (2.7)			
30 cm	4.5 (677)	2.0 (27)	1.7 (1.2)	6.5 (678)	3.9 (28)	3.5 (1.6)			
100 cm	1.4 (179)	0.6 (8.2)	0.5 (0.2)	2.0 (179)	1.2 (8.3)	1.1 (0.2)			

Table 10: Scenario 2

100  $\mu\text{Sv/h}$  then the ensemble would be considered *radioactive* and, if extraction were necessary for maintenance, would need to be stored in a ‘controlled’ area [15]. Otherwise, for dose rates less than 10  $\mu\text{Sv/h}$ , the ensemble could be stored simply in a ‘supervised’ area [15].

## 4.2 Low mass power tapes

It is intended to use low-mass power tapes running between the SCT patch-panels PPB1 and each of the 1056 modules comprising a half-barrel. The composition of the tape is  $\sim 35\%$  Aluminium and  $\sim 65\%$  Kapton/Glue, with a mass  $\sim 0.1 \text{ g/cm}$ . This gives a total mass of  $\sim 7.5 \text{ kg}$  between each barrel-end and PPB1. The results of the calculations given in Section 2 indicate that  $^{22}\text{Na}$  production in Aluminium (via spallation) will be the radionuclide of most interest. The importance of  $^{22}\text{Na}$  production in the power-tapes can be obtained by comparing the mass of Aluminium in the tapes ( $\sim 2.6 \text{ kg}$ ) with the mass of target material in the modules responsible for  $^{22}\text{Na}$  production (mainly Silicon + Aluminium). According to Table 1, there is some  $\sim 15.8 \text{ kg}$  of Aluminium + Silicon in a half-barrel. However, a more appropriate comparison is to take only the end-modules as they approximate better the geometrical region of interest, in which case there is  $\sim 2.6 \text{ kg}$  of Aluminium + Silicon. Therefore, similar amounts of  $^{22}\text{Na}$  will be produced in the end-modules as in the low-mass power tapes and similar dose rates can be expected as predicted for the module-ensemble.

## 4.3 Cooling

The cooling material between PPB1 and the barrel-ends currently comprise: inlet-tubes (copper-nickel); outlet-tubes (aluminium-alloy); exhaust manifolds and inlet-unions (aluminium-alloy with nickel and copper plating). In total, for each barrel-end, this gives approximately  $\sim 2.2 \text{ kg}$  of aluminium-alloy (94.3% Al, 0.4% Si, 0.4% Fe, 0.1% Cu, 0.4% Mn, 4.0% Mg, 0.05% Cr, 0.25% Zn, 0.15% Ti),  $\sim 1.2 \text{ kg}$  Cu and  $\sim 0.6 \text{ kg}$  Ni. The effect of this material on dose-rates from the barrel system can be obtained in the same spirit as was done for the power tapes by assigning the cooling material mass to the end-modules of the barrel system. This gives  $\sim 12.5 \text{ g}$ ,  $\sim 6.8 \text{ g}$  and  $\sim 3.4 \text{ g}$  of Al-alloy, Cu and Ni per module respectively. The quantity of Al is similar to the Al + Si content in the module so similar contributions to dose rates from  $^{22}\text{Na}$  can be expected. Also of interest is  $^{64}\text{Cu}$ , the results given in Section 2 indicate that dose rates from  $^{64}\text{Cu}$  ( $t_{1/2} = 12.7\text{h}$ ) dominate on timescales of a few days assuming  $\sim 2.6 \text{ g}$  of Cu per module. The only other elements of



radiological interest are  $^{65}\text{Zn}$  ( $t_{1/2} = 243.8\text{d}$ ) and  $^{51}\text{Cr}$  ( $t_{1/2} = 27.7\text{d}$ ), which were not considered in the calculations of Section 2. However, the quantity of Chromium is small and  $^{51}\text{Cr}$  decays primarily through electron-capture with no associated gammas and can be ignored.  $^{65}\text{Zn}$  has a similar half-life as  $^{110\text{m}}\text{Ag}$  but a lower thermal neutron capture cross-section. The amount of Zinc is small in the current material estimates and dose-rates from Silver will dominate, however care should be taken to ensure that the amount of Zinc does not increase dramatically.

#### 4.4 Comments concerning PPB1 and beyond

No attempt has been made to investigate the activation of PPB1 and beyond. The reason for this is three-fold: First, the focus of this study has been to investigate, in detail, the activation of barrel-modules and assess their radiological impact. Secondly, there are significant uncertainties in the elemental composition of patch-panels etc. which will make any predictions unreliable. Indeed, for low-energy neutron activation the best strategy would be to irradiate samples as was done for the hybrids. Finally, it does not make sense to consider the PPB1-and-beyond services independent of nearby ATLAS sub-systems, services, supports etc., especially from an access and maintenance point of view. It should be noted, however, that on this latter point a lot of effort is going into assessing the general activation picture for ATLAS and these studies are now quite advanced [18].

### 5 Discussion

The activation estimates described in Section 2 conclude that individual SCT barrel-modules will fall into the *slightly-radioactive* category, after several years of LHC operation and several weeks cool-down time. The irradiation measurements described in Section 3 have shown that module-hybrids, irradiated with low-energy neutrons to fluences in excess of those expected over the lifetime of the SCT, are in the *slightly-radioactive* category after several weeks cool-down time. The hybrid irradiations have also shown that the dominant isotopes contributing to hybrid-activity from neutron-capture reactions, after several weeks cool-down time, are  $^{110\text{m}}\text{Ag}$  and  $^{198}\text{Au}$ , as predicted in the low-energy neutron calculations of Section 2. Importantly, the quantity of silver and gold assumed in the calculations has been reasonably estimated<sup>†</sup>, giving confidence in module-activity predictions. However, the possible existence of the measured elements not included in the hybrid material-inventory of Table 1, albeit in small quantities, highlights the limits of activation estimates from neutron capture. In addition, the unexpected presence of cobalt will ensure that the modules remain *slightly-radioactive* for many years after LHC shutdown.

While much effort has been given to understanding low-energy neutron activation of module components, the dominant contribution to  $\gamma$  dose rates is predicted to come from  $^{22}\text{Na}$ , produced in high-energy spallation reactions. Dose rates from  $\gamma$ s are usually more important than  $\beta$  dose rates as the latter are easier to shield against.

---

<sup>†</sup>The mass of silver and gold in the hybrid is measured (estimated) to be 74mg (160mg) and 14mg (10mg) respectively.



Concerning dose rates from the barrel system, it has been shown in Section 4 that the contribution from the module material should not create any serious problems. The  $\beta$ -doses are high during the first few days, due to  $^{64}\text{Cu}$ , but access on this timescale is unlikely and the total dose-rates soon fall to less than  $100\ \mu\text{Sv/h}$  at 10 cm. After several weeks the total dose-rates are likely to be less than  $10\ \mu\text{Sv/h}$  at 10 cm. As for general access and maintenance scenarios, dose-rates at distances of  $\sim 1\text{ m}$  are more relevant and after several days cool-down time dose-rates from the modules are unlikely to be more than a few  $\mu\text{Sv/h}$ . It was also argued in Section 4 that similar contributions can be expected from the barrel-end cooling and power-tape services. However, dose rates from the barrel material and barrel-end services will be small when compared with other elements of the ATLAS experiment [18]. Dose rates from SCT-system material not considered in this report (eg patch-panels and associated cabling) may well be significant due to the large increase in system mass and this needs to be checked, but within the framework of the overall ATLAS activation situation.

A final comment concerns the eventual storage or disposal of the SCT modules at the end of the detector lifetime. According to the work presented in this report, the dominant radionuclides after 10 years cool-down time will be  $^3\text{H}$ ,  $^{22}\text{Na}$  and  $^{60}\text{Co}$ . Extending the results given in Table 4, the corresponding specific-activities will be  $69\text{ Bq/g}$ ,  $4\text{ Bq/g}$  and  $0.5\text{ Bq/g}$  respectively. These can be compared with the CERN exemption limits [15] of  $300\text{ Bq/g}$ ,  $3\text{ Bq/g}$  and  $1\text{ Bq/g}$ . However, the results of hybrid irradiation show some  $4\text{ mg}$  of  $^{60}\text{Co}$  not accounted for in the calculations of Section 2, giving a total module specific activity due to  $^{60}\text{Co}$  of  $\sim 2.5\text{ Bq/g}$ . After a 15 years cool-down period it is likely that the module specific activities will be below the CERN exemption limits.

## References

- [1] I.Dawson, Review of the Radiation Environment in the Inner Detector, ATL-INDET-2000-006
- [2] SCT Barrel Module, Final Design Reviews: SCT-BM-FDR-1, SCT-BM-FDR-2, SCT-BM-FDR-3 and SCT-BM-FDR-4. Available from: [http://atlasinfo.cern.ch/Atlas/GROUPS/INNER\\_DETECTOR/SCT/module/SCTbarrelmod.html](http://atlasinfo.cern.ch/Atlas/GROUPS/INNER_DETECTOR/SCT/module/SCTbarrelmod.html)
- [3] Table of material for the Cu/Polyimide hybrid 12  $\mu\text{m}$  Copper, version 4. Available from: [http://jsdhp1.kek.jp/~unno/si\\_hybrid/k4/KhybridXo01feb26.pdf](http://jsdhp1.kek.jp/~unno/si_hybrid/k4/KhybridXo01feb26.pdf)
- [4] Private communication, T.Weidberg
- [5] T.Niinikoski, Evaporative Cooling - Conceptual Design for ATLAS SCT, ATL-INDET-98-214
- [6] Evaluated Nuclear Data Files (ENDF), obtained from: <http://www-nds.iaea.org/ndsstart.html>
- [7] Chart of the Nuclides, produced by Knowles Atomic Power Laboratory; 14th edition - revised to April 1988. (Using National Nuclear Data Center (NNDC) files.)
- [8] A.Fasso, A.Ferrari, J.Ranft and P.Sala, Full details can be found at FLUKA official website; <http://fluka.web.cern.ch/fluka/>
- [9] A.Ferrari and P.Sala, The Physics of High Energy Reactions, ATLAS Internal note, PHYS-NO-113, 1997
- [10] R.Engel and J.Ranft, *Hadronic photon-photon interactions at high-energies*, Physics. Rev. D54:4244-4262, 1996
- [11] K.Potter and G.Stevenson, *Average Interaction Rates for Shielding Specification in High Luminosity LHC Experiments*, CERN AC/95-01, CERN/TIS-RP/IR/95-05.
- [12] K.J.Connor and I.S.McLintock, *Radiation Protection*, HHSC Handbook No. 14, 1997, ISBN 0-94237-21-X
- [13] I.S.McLintock, *Bremsstrahlung from Radionuclides*, HHSC Handbook No. 15, 1994, ISBN 0-948237-23-6
- [14] M.Barbier, *Induced Radioactivity*, North-Holland publishing company, 1969, SBN 7204-0145-3
- [15] Radiation Safety Manual, CERN – TIS/RP, 1996
- [16] For details, see: <http://www-f9.ijs.si/~mandic/ReacSetup.html>
- [17] R. Jeraj et al., *Monte Carlo Characterization of Irradiation Facilities in the TRIGA Reactor Core*, Nuclear Energy in Central Europe 2001, Portorož, Slovenia, 2001 <http://www.drustvo-js.si/port2001>
- [18] V. Hedberg, *ATLAS activation studies*, <http://atlasinfo.cern.ch/Atlas/TCOORD/Activities/CommonSys/Shielding/Activation/activation.html>